The Crystal Structure of AMP-Bound PDE4 Suggests a Mechanism for Phosphodiesterase Catalysis[†,‡]

Qing Huai,[§] John Colicelli,[||] and Hengming Ke*[,§]

Department of Biochemistry and Biophysics and Lineberger Comprehensive Cancer Center, The University of North Carolina, Chapel Hill, North Carolina 27599-7260, and Department of Biological Chemistry and Molecular Biology Institute, University of California at Los Angeles School of Medicine, Los Angeles, California 90095-1737

Received April 25, 2003; Revised Manuscript Received September 15, 2003

ABSTRACT: Cyclic nucleotide phosphodiesterases (PDEs) regulate the intracellular concentrations of cyclic 3′,5′-adenosine and guanosine monophosphates (cAMP and cGMP, respectively) by hydrolyzing them to AMP and GMP, respectively. Family-selective inhibitors of PDEs have been studied for treatment of various human diseases. However, the catalytic mechanism of cyclic nucleotide hydrolysis by PDEs has remained unclear. We determined the crystal structure of the human PDE4D2 catalytic domain in complex with AMP at 2.4 Å resolution. In this structure, two divalent metal ions simultaneously interact with the phosphate group of AMP, implying a binuclear catalysis. In addition, the structure suggested that a hydroxide ion or a water bridging two metal ions may serve as the nucleophile for the hydrolysis of the cAMP phosphodiester bond.

Cyclic 3′,5′-adenosine and guanosine monophosphates (cAMP[1] and cGMP, respectively) are intracellular second messengers that mediate the response of cells to a wide variety of stimuli, primarily through the activation of cyclic nucleotide-activated protein kinases. Regulation of cAMP and cGMP concentrations in vivo is essential for many physiological processes, such as cardiac and smooth muscle contraction, glycogenolysis, platelet aggregation, ion channel conductance, apoptosis, growth control, and neurological function (*1*−*6*). Cyclic nucleotide phosphodiesterases (PDEs) are enzymes that hydrolyze cAMP and cGMP and are essential for the regulation of cyclic nucleotide concentrations in the cell (*7*−*9*).

The human genome encodes 21 PDE genes categorized into 11 families (*6*−*17*). Additional diversity is generated through the alternate splicing of PDE mRNAs, producing more than 60 PDE isoforms in various human tissues. Family-selective inhibitors of PDEs constitute a rapidly growing class of pharmaceuticals directed against several diseases. These drugs have shown varying degrees of efficacy as cardiotonic agents, vasodilators, smooth muscle relaxants, antidepressants, antithrombotics, antiasthmatics, and agents for improving cognitive functions such as memory (*18*−*25*). For example, the PDE5 inhibitor sildenafil (Viagra) has proven to be effective as a drug for male erectile dysfunction, and the PDE3 inhibitor cilostazol (Pletal) is a drug for the reduction of symptoms of intermittent claudication. Selective inhibitors of PDE4 form the largest group of inhibitors for any PDE family, and have been studied as anti-inflammatory drugs targeting asthma and chronic obstructive pulmonary disease (*20*, *26*−*28*).

All PDE enzymes contain a conserved catalytic domain of approximately 300 amino acids, suggesting that diverse PDE enzymes share a conserved active site structure and enzymatic mechanism. However, each PDE family has its own substrate preference and kinetic signature for cAMP and cGMP, and each has a unique inhibitor specificity profile.

Table 1: Diffraction Data and Structure Refinement Statistics for the PDE4D−AMP Structure

data collection	
space group	$P2_12_12_1$
unit cell dimensions [*a*, *b*, *c* (Å)]	99.2, 111.2, 159.7
resolution (Å)	2.4
total no. of measurements	404282
no. of unique reflections	64052
completeness (%)	91.8 (87.9)[a]
average I/σ	21.9 (5.3)
R_{merge}	0.075 (0.45)
structure refinement	
R-factor	0.229
R_{free}	0.274
no. of reflections	67124[b]
rms deviation	
bonds (Å)	0.0066
angles (deg)	1.18
average *B*-factor (Å^2)	
all atoms	50.3
protein (1336 residues)	50.4
AMP (four molecules)	56.2
Zn1 (four atoms)	42.0
Zn2 (four atoms)	65.9
water (86 molecules)	34.0

[a] The numbers in parentheses are for the 2.4−2.5 Å resolution shell. [b] The structure refinement included 6941 unique reflections between 2.4 and 2.3 Å resolution.

[†] This work was supported in part by NIH Grants GM59791 to H.K. and NS31911 to J.C.

[‡] The coordinates have been deposited in the Protein Data Bank as entry 1PTW.

* To whom correspondence should be addressed. Phone: (919) 966-2244. Fax: (919) 966-2852. E-mail: hke@med.unc.edu.

[§] The University of North Carolina.

[||] University of California.

[1] Abbreviations: PDE, cyclic nucleotide phosphodiesterases; cAMP, cyclic 3′,5′-adenosine monophosphate; cGMP, cyclic 3′,5′-guanosine monophosphate.

10.1021/bi034653e CCC: $25.00 © 2003 American Chemical Society
Published on Web 10/25/2003

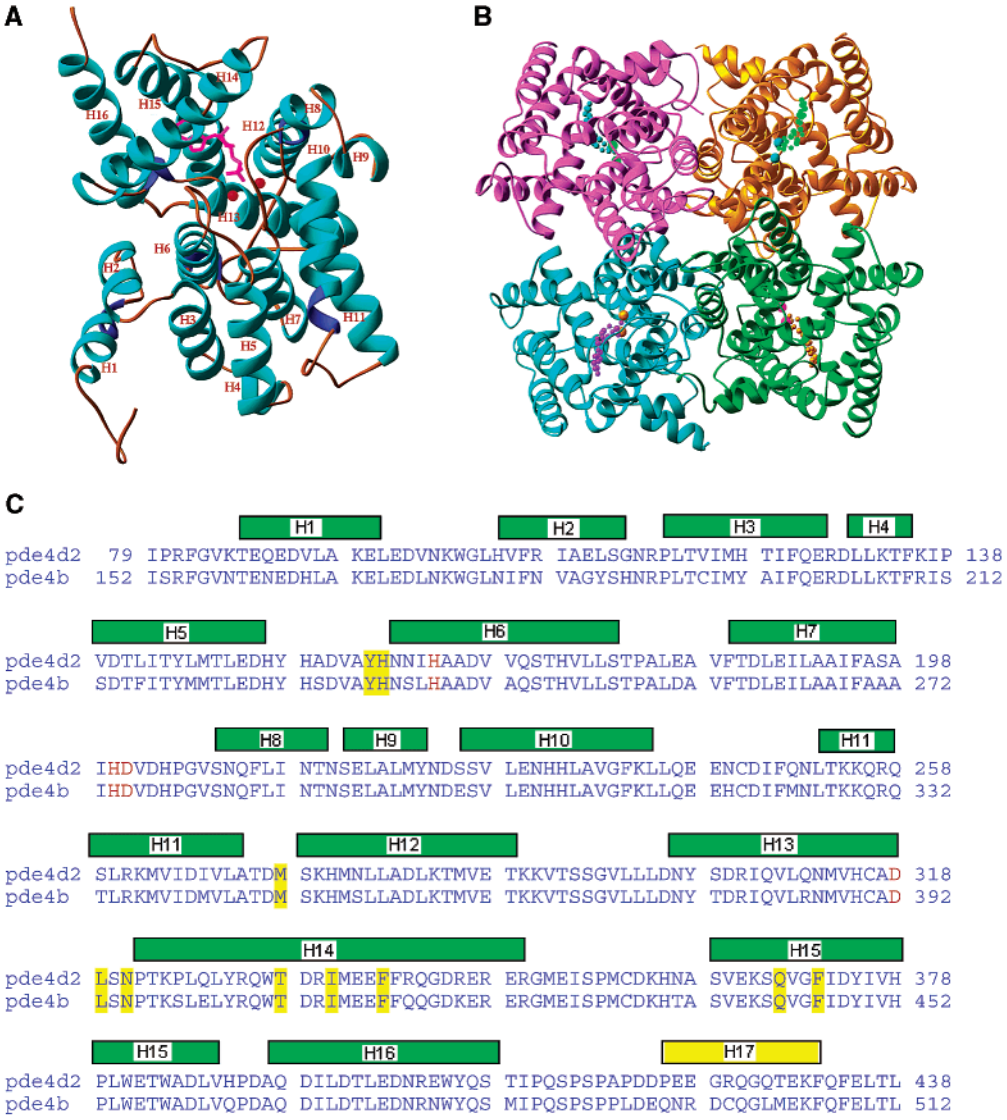

FIGURE 1: Catalytic domain of PDE4D2. (A) Ribbon diagram of monomeric PDE4D2. AMP is shown as magenta sticks, while two divalent metals are shown as red balls. (B) Tetramer of PDE4D2. Color codes are magenta for subunit A, gold for B, cyan for C, and green for D. (C) Sequences of the catalytic domain of PDE4. The metal binding residues (His164, His200, Asp201, and Asp318) are shown in red, while the AMP binding residues are highlighted with yellow. The green bars represent helices common for both PDE4D2 and PDE4B. The yellow bar is the helix found in only PDE4B.

The PDE4, -7, and -8 family members preferentially hydrolyze cAMP, while PDE5, -6, and -9 are cGMP specific. PDE1, -2, -3, -10, and -11 enzymes exhibit activity toward both substrates but have distinct K_m values for cAMP and cGMP. Despite extensive analysis, however, the mechanism of hydrolysis has not been elucidated for any PDE. We report here the crystal structure of the catalytic domain of human PDE4D2 in complex with AMP, the product of catalysis, at 2.4 Å resolution. The structure suggests a binuclear catalysis mechanism for hydrolysis of the cyclic nucleotide phosphodiester bond.

EXPERIMENTAL PROCEDURES

Protein Expression and Purification. The EST (expressed sequence tag) cDNA clones of PDE4D2 (BF059733) were purchased from ATCC and subcloned following standard methods. The coding region for amino acids 79−438 of PDE4D2 was amplified by PCR and subcloned into expression vector pET15b. The resulting plasmid pET-PDE4D2 was transformed into *Escherichia coli* strain BL21 (Codonplus) for overexpression. The *E. coli* cell carrying pET-PDE4D2 was grown in LB medium at 37 °C to an absorption A_{600} of 0.7, and then 0.1 mM isopropyl β-D-thiogalactopyranoside was added prior to further growth at 12 °C for 40 h. The recombinant PDE4D2 was purified with Ni−NTA affinity (Qiagen), thrombin cleavage, Q-Sepharose (Phamacia), and Superdex 200 (Phamacia) columns. The PDE4D2 protein was more than 95% pure as shown via SDS−PAGE. A typical purification yielded more than 100 mg of PDE4D2 from a 2 L cell culture.

Crystallization and Data Collection. The crystals were grown by vapor diffusion against a well buffer of 50 mM HEPES (pH 7.5), 15% PEG3350, 25% ethylene glycol, 5% methanol, and 5% DMSO at 4 °C. The protein drop was prepared by mixing 10 mM cAMP and 0.4 mM zinc sulfate with 15 mg/mL PDE4D2 in a storage buffer of 50 mM NaCl, 20 mM Tris-HCl (pH 7.5), and 1 mM β-mercaptoethanol for the crystallization. To saturate the cAMP binding, the

crystals were soaked in a buffer of 50 mM HEPES (pH 7.5), 20% PEG3350, 25% ethylene glycol, 0.4 mM zinc sulfate, and 50 mM cAMP at room temperature for 5 h and then immediately dipped into liquid nitrogen. The crystals of PDE4D2 belong to space group $P2_12_12_1$ with the following cell dimensions: $a = 99.2$ Å, $b = 111.2$ Å, and $c = 159.7$ Å. The diffraction data were collected on beamline 14C of APS at Argonne National Laboratory (Argonne, IL) (Table 1) and processed with HKL (*29*).

Structure Determination. The structure of PDE4D2 in complex with AMP was determined by the direct application of the tetramer of the PDE4D2−rolipram structure to the crystal system (*30*). The orientation of the individual subunits in the PDE4D2−AMP tetramer was optimized by rigid-body refinement in CNS (*31*), yielding *R*-factor and R_{free} values of 0.355 and 0.352, respectively, for 67 124 reflections up to 2.3 Å resolution. To minimize the model biases, the electron density map was improved by the solvent flattening and local symmetry averaging in the density modification package of CCP4 (*32*). The atomic model was rebuilt against the improved electron density map with O (*33*) and refined with CNS (Table 1).

RESULTS AND DISCUSSION

The PDE4D2 Catalytic Domain Adopts a Tetrameric Structure. Four molecules of the AMP-complexed PDE4D2 catalytic domains were tightly associated into a tetramer in the crystal (Figure 1), while a monomeric form was observed for uncomplexed PDE4B (*34*). The monomer of the catalytic domain of PDE4D2 (amino acids 79−438) contains 16 α-helices with the same folding as PDE4B (*34*). The electron density revealed the trace of residues 86−412. N-Terminal residues 79−85 had partial electron density for subunits A and D, but no observable electron density for subunits B and C. Residues 413−438 of PDE4D2 could not be traced due to a lack of electron density and presumably existed in a random conformation. This is in contrast to a helix conformation of residues 496−508 in PDE4B, which correspond to residues 422−434 of PDE4D2. A native PAGE showed three major bands of the catalytic domain of PDE4D2, that apparently correspond to monomeric, dimeric, and tetrameric states in solution. Since the structural study showed that cAMP was converted to AMP during the crystallization (see the discussion below), the PDE4D2 tetramer appears to be an active form of the enzyme.

The superposition of the PDE4D2 subunits in the tetramer shows an average root-mean-squared deviation of 0.59 Å for the backbone atoms of the four subunits, indicating an overall structural similarity among the subunits. Comparison among the four active sites in the tetramer of the PDE4D2 catalytic domains detected no significant changes in the conformations of the active site residues. However, significant variations in local conformations were observed for certain loops in the PDE4D2 tetramer. A shift of up to 3.4 Å, ∼5 times the average, was observed for the backbone atoms of the Val292−Ser295 loop. Since this loop is far from the active site of the enzyme, any impact on catalysis would need to be indirect and allosteric. In addition, the averaged *B*-factors of 58.3 and 55.2 Å^2 for subunits B and C, respectively, are significantly higher than the values of 45.9 and 42.2 Å^2 observed for subunits A and D, respectively. Since a crystallographic *B*-factor is a scale of thermal movement of atoms in crystals, the higher *B*-factors imply relative conformation flexibility of subunits B and C. The implication of these variations in the PDE4D2 tetramer is not clear, but may reflect the contribution of allosteric regulation in PDE4 catalysis.

Table 2: Interfacial Interactions in the PDE4D2−AMP Structure

	distances (Å)
hydrogen bonds between	
chains A and C or B and D	
Arg116 NE···Glu349 OE2	2.77, 3.45, 3.37, 3.00
Arg116 NH2···Glu349 OE1	2.74, 3.33, 2.43, 2.65
Arg116 NH2···Glu349 OE2	3.15, 3.52, 2.90, 3.06
Asp151 OD1···Arg346 NH1	2.63, 3.10, 2.78, 3.21
Asp151 OD1···Arg350 NH2	2.90, 3.37, 3.13, 2.70
Thr215 O···Glu244 N	2.82, 2.80, 2.94, 2.80
Asn216 ND2···Glu244 OE1	2.98, 2.63, 2.87, 3.04
Arg350 NH1···Thr148 OG1	3.00, 3.38, 2.78, 3.50
Arg350 NH2···Thr148 OG1	3.20, 2.90, 3.35, 3.64
hydrogen bonds between	
chains A and B or C and D	
Asn214 O···Lys254 NZ	2.78, 4.05, 2.84, 6.78
Asn214 OD1···Gln258 NE2	4.60, 2.80, 2.96, 5.98
Asn216 OD1···Lys254 NZ	2.76, 3.24, 2.97, 2.97
Tyr223 OH···Met222 O	2.79, 3.45, 3.56, 2.83
Asn224 ND2···Asn231 OD1	2.90, 2.92, 3.05, 2.73
Asn224 ND2···Asn231 O	3.00, 3.46, 3.97, 3.05
Asp225 OD1···Arg261 NH2	3.23, 3.34, 2.93, 4.95
Asp225 OD2···Arg261 NE	2.61, 2.68, 2.99, 3.09
Asp225 OD2···Arg261 NH2	3.26, 3.46, 3.37, 3.44
hydrogen bonds between	
chains A and D or B and C	
Glu244 OE1···Lys254 NZ	3.03, 2.75, 2.96, 2.63
Glu244 OE1···Arg257 NH1	2.96, 2.97, 6.40, 4.99
Glu244 OE2···Arg257 NH2	2.78, 2.82, 7.60, 5.68
van der Waals interactions between	
chains A and C or B and D	
Asn214···Glu244	
Thr215···Glu244, Glu243	
Asn216···Glu243, Glu244, Lys254	
Glu218···Lys239	
Ala220···Arg261	
Arg346···Asp151	
Glu349···Arg116, Met147	
Arg350···Thr148, Asp151	
van der Waals interactions between	
chains A and B or C and D	
Leu221···Arg261	
Met222···Tyr223	
Asn224···Asn231, Leu234, Arg261, Ile265	
Asp225···Arg261	
Ala235···Asn224	
Gln242···Leu221	
Lys254···Asn214, Asn216	
Gln258···Asn214	
van der Waals interactions between	
chains A and D or B and C	
Lys239···Gln242	
Glu244···Lys254, Arg257	

Hydrogen bonds are the major forces stabilizing the PDE4D2 tetramer (Table 2 and Figure 1). The interfacial interactions between subunits A and B or between subunits C and D involve the residues from helices H8−H11. The interface between subunits A and C or between subunits B and D is formed with the residues of helices H3, H8, H10, and H14. Subunit A also contacts subunit D via H11, and the same was seen for the interaction of B and C (Table 2). The C-terminal residues after position 413 of PDE4D2 could not be traced in the electron density of the crystals. However,

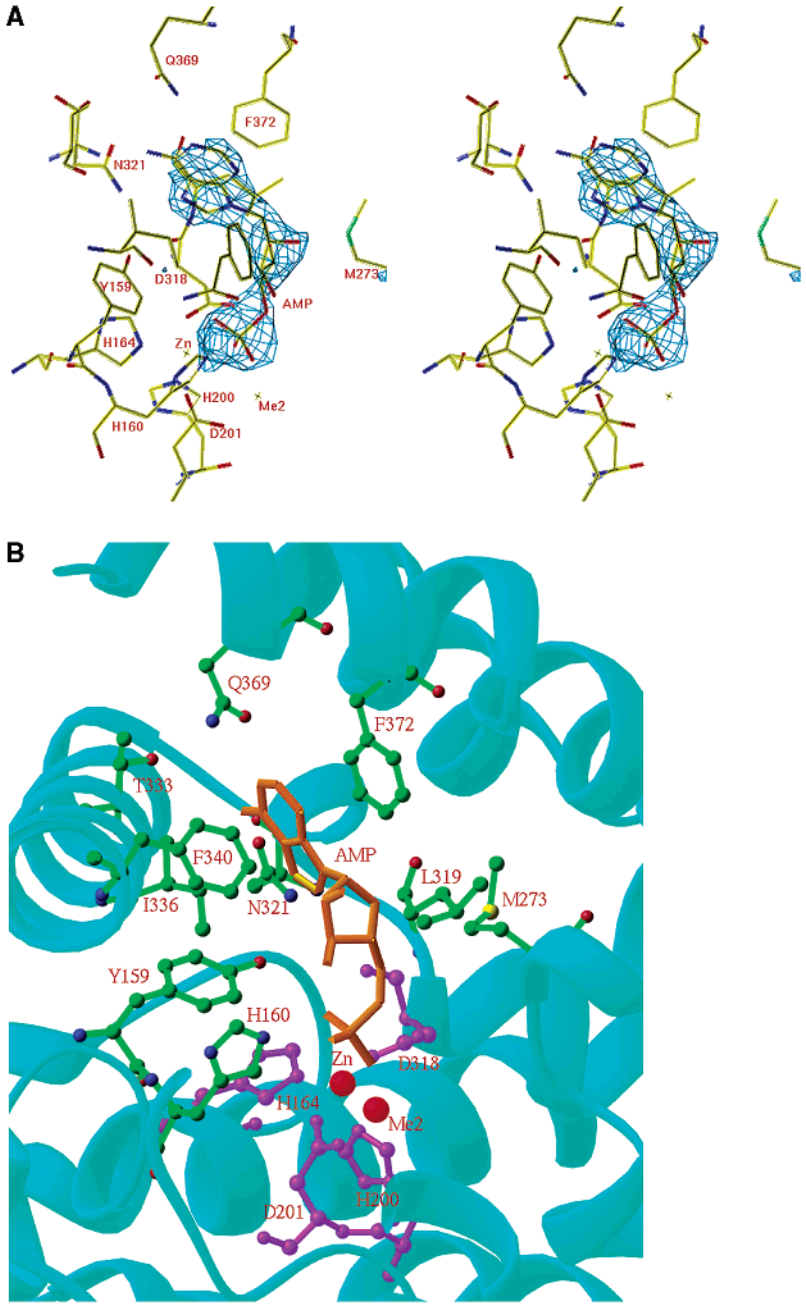

FIGURE 2: AMP binding. (A) Stereoview of electron density for AMP, which was calculated from the omitted $F_o - F_c$ map and contoured at 3.5σ. (B) Interactions of AMP with the active site residues. The metal binding residues are shown in purple.

the position of helix H16 (residues 392−410) indicates that the C-terminus points outside of the tetrameric body, implying a potential regulatory role for these residues. Further support for a regulatory function of the C-terminus comes from the observation that the C-terminal helix (residues 496−508) of one molecule interacts with the active site of another molecule in the PDE4B structure (*34*). This finding appears to conflict with a model that proposes a role for the C-terminus of PDE4 in dimerization (*6*).

AMP Binding. Electron density analysis revealed that the active site of PDE4D2 was occupied by the reaction product 5′-AMP (Figure 2), although cAMP was used in the crystallization. One molecule of AMP was bound to each active site of the tetramer in a similar pattern (Table 3). The AMP phosphate group exhibited a direct interaction with both metal ions and formed hydrogen bonds with His160, Asp201, and Asp318 (Table 3). The AMP phosphate also resides 3.2−4.0 Å from residues Tyr159, His164, and His200. The adenine group of AMP adopts an *anti* conformation and orients to the hydrophobic pocket made up of residues Tyr159, Leu319, Asn321, Thr333, Ile336, Gln369, and Phe372. It forms three hydrogen bonds with Gln369 and Asn321 and stacks against Phe372. The ribose of AMP has a configuration of C3′-*endo* puckering and makes van der Waals contacts with PDE residues His160, Met273, Asp318, Leu319, Ile336, Phe340, and Phe372.

The AMP binding as observed in the PDE4D2−AMP structure is consistent with the docking model of cAMP in the catalytic pocket of PDE4 (*34*, *35*) and is also supported by results from site-directed mutagenesis. Mutations of residues His160, His164, His200, Thr333, Ile336, Phe340, and Phe372 in enzymes of the PDE4 subfamilies reduced

Table 3: Interactions of AMP with the Active Site Residues of PDE4D2

Hydrogen Bonds and Metal Coordinations		
AMP atom	PDE4D atom	distance (Å)[a]
O′	His160 NE2	3.21, 3.18, 2.37, 2.78
	water W5	2.51, 2.88, 3.66
OL	His160 NE2	2.50, 3.06, 3.18, 2.80
	Zn2	3.02, 2.75, 2.38, 3.04
	water W3	2.75, 3.33, 2.67, 2.61
OR	Asp201 OD2	3.01, 3.27, 2.72, 2.73
	Asp318 OD2	2.85, 2.66, 2.91, 3.03
	Zn2	2.41, 2.46, 3.13, 2.45
	Zn1	2.32, 2.38, 2.17, 2.29
	water W4	3.33, 3.27, 3.30, 3.82
N1	Gln369 NE2	2.86, 3.26, 3.05, 3.22
N6	Asn321 OD1	2.82, 2.76, 2.88, 2.90
N7	Asn321 ND2	3.31, 3.35, 3.13, 2.97
	van der Waals Contacts	
phosphate	Tyr159, His160, His164, His200, Asp201, Asp318	
ribose	His160, Met273, Asp318, Leu319, Ile336, Phe340, Phe372	
base	Tyr159, Leu319, Asn321, Thr333, Ile336, Gln369, Phe372	

[a] The four numbers represent the hydrogen bond distances in the four PDE4D2 subunits.

or even abolished catalytic activity (*35*−*40*). It is also interesting to note that mutations of the corresponding AMP binding residues in other PDE families dramatically reduced the catalytic activity. For example, mutations of PDE3A residues Tyr751 (Tyr159 in PDE4D2), Asp950 (Asp318), Phe972 (Phe340), and Phe1004 (Phe372) resulted in a 15−280-fold loss of catalytic activity (*41*). For bovine PDE5A, a mutation of Glu672 (Glu230 in PDE4D2 and completely conserved in all PDE family members) yielded a significant reduction in k_{cat} (*42*).

Metal Binding. Two metal ions reside in the active site of PDE4D2, the same as previously reported for the PDE4B structure (*34*). The $2F_o - F_c$ map revealed two strong peaks: $\sim 10\sigma$ for the first metal site and $\sim 6\sigma$ for the second site. These sites are separated by ~3.8 Å. The metal binding to the protein residues in the AMP-bound PDE4D2 structure is similar to that in the unliganded PDE4B (*34*), except for the direct interactions of the metals with AMP. Each metal ion forms six coordinations with protein residues, AMP, and water molecules in a distorted octahedral configuration. The first metal coordinates with His164, His200, Asp201, Asp318, and two phosphate oxygen atoms of AMP (Figure 3). The second metal coordinates with Asp318, two phosphate oxygen atoms of AMP, and three bound water molecules. The first metal in the PDE4B structure was assigned as a zinc ion on the basis of the metal coordinations, anomalous scattering behavior, and biochemical evidence (*34*). This is supported by the absorption spectra of the PDE4D2 crystals at the wavelength of the zinc absorption edge. In addition, four strong peaks at $6-9\sigma$ were observed in the anomalous difference Fourier map calculated from the refined structure and the PDE4D2−AMP data set that was measured at a wavelength of 0.9 Å. These peaks correspond to the first metal sites in the PDE4D2 tetramer, thus confirming the existence of the strongly bound metals. The assignment for the second metal is difficult because of its relatively loose binding. We used zinc as the second metal in the structure refinement because the crystallization buffer contained 0.4 mM zinc sulfate. However, the physiological metal for the catalysis is not clear. It could be magnesium or another divalent ion, as suggested by biochemical studies showing that zinc at 1 μM or other divalent metals such as Mn^{2+}, Co^{2+}, Ni^{2+}, and Mg^{2+} at 2−100 μM activate catalysis by PDEs (*43*−*45*).

The first metal site was previously proposed to play both structural and catalytic roles because it conjoins the residues from three subdomains of PDE4B and constitutes a physical component of the active site (*34*). Indeed, the structure of the PDE4D2−AMP complex reveals that this metal ion forms two coordinations with the phosphate group, thus confirming its catalytic role (Figure 3). The observation that both metals coordinate with the phosphate group of AMP suggests a binuclear mechanism in which the hydrolysis of cAMP/cGMP is jointly accomplished by two divalent metals. This type of binuclear catalysis would be similar to the proposed mechanism of phosphoester bond hydrolysis performed by protein phosphatases such as calcineurin (*46*, *47*).

The designation of zinc ion as an occupant of the first metal site in the crystal structures of unliganded PDE4B and the PDE4D2−AMP complex is further supported by the high degree of similarity between two conserved $HX_3HX_{24-26}E$ sequences of PDE and the sequences of known zinc binding enzymes (*48*). However, two $HX_3HX_{24-26}E$ motifs jointly form a single pocket for binding of both metal ions in the crystal structures of PDE4B (*34*) and PDE4D2, instead of each motif binding an individual metal ion, as one might predict on the basis of other zinc enzymes. There is some inconsistency regarding the number of zinc atoms reported to be at the active sites in different PDE family members: one Zn^{2+} site per PDE4A monomer (*45*), two Zn^{2+} ions for *Vibrio fischeri* PDE (*49*) and for PDE4A (*50*), and three Zn^{2+} ions for PDE5 (*44*). However, the absolute conservation of the metal binding residues across the PDE families and no evidence of any additional metal binding pockets as shown by the crystal structures suggest a universal mechanism of binuclear catalysis for all PDEs.

Tentative Mechanism of Cyclic Nucleotide Catalysis by PDEs. The hydrolysis of a phosphodiester bond requires a nucleophilic attack by a water molecule or a hydroxide ion (*51*, *52*). In the crystal structures of unligated PDE4B (*34*) and PDE4D2 (unpublished results), a water molecule or hydroxide ion bridges two metal ions and also forms a hydrogen bond with Asp318. This water or hydroxide ion is a most likely candidate for carrying out the nucleophilic attack on the phosphorus atom. In this model, the phosphate group of cAMP may form hydrogen bonds with His160 and interact with one or both metal ions (Figure 4). These interactions polarize the phosphodiester bond and confer a partial positive charge to the phosphorus atom. Asp318 serves as a general base to activate the bridging water or hydroxide ion for nucleophilic attack. Asp201 that coordinates both metal ions may also contribute to the activation because of its proximity to the nucleophile. His160, which is ~4 Å away from O3′ of AMP in the PDE4D2−AMP structure, may donate a proton to O3′ for the completion of phosphodiester bond hydrolysis (Figure 4). Although the structure cannot differentiate a water molecule and hydroxide ion, the nucleophile is likely a hydroxide ion, as proposed for the binuclear catalysis of dihydroorotase (*53*) and other enzymes

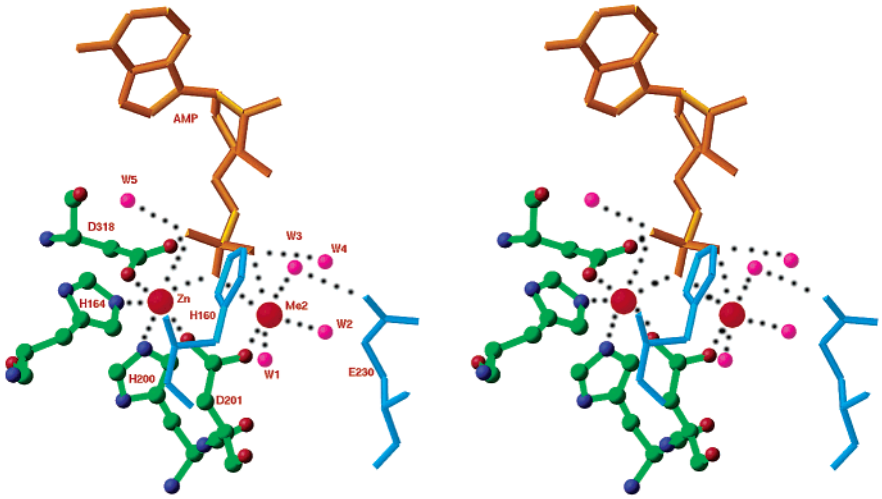

FIGURE 3: Interactions of the metal ions. The golden sticks represent AMP. Cyan sticks are His160 and Glu230. Dotted lines represent the interactions involving the metals and AMP. Me2 represents the second metal.

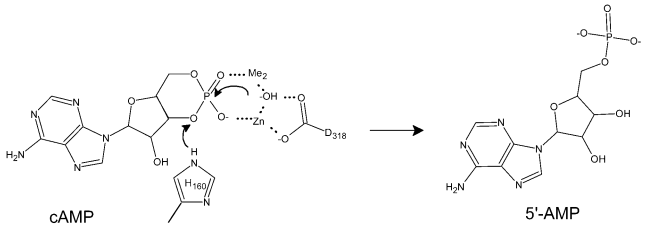

FIGURE 4: Tentative mechanism for the hydrolysis of the cAMP phosphodiester bond by PDE4. Magnesium represents the putative second metal labeled Me2 in Figure 1.

(*51*, *52*). When incorporation of the attacking nucleophile into the product of hydrolysis is considered, this model is supported by the fact that this water or hydroxide is displaced by the phosphate oxygen of AMP in the PDE4D2−AMP structure. The position of the bridging nucleophile relative to AMP would lead to an inversion of configuration at phosphorus. Such an inversion has been proposed as a feature of cAMP hydrolysis (*54*, *55*). A similar mechanism was proposed on the basis of the model binding of cAMP to PDE4 (*56*).

On the other hand, we could not exclude the possibility that water molecule W3 serves as an alternative nucleophile. Water W3 is coordinated with the second metal ion and forms hydrogen bonds with the side chain OE2 atom of Glu230, the carbonyl oxygen of Thr271, and a phosphate oxygen of AMP (Figure 3). Thus, Glu230 may serve as a general base to activate water W3 for the nucleophilic attack on the phosphorus atom, while His160 serves as a general acid to donate a proton to O3′. The proposed roles of Glu230 and His160 are supported by the absolute conservation of both residues across all members of the PDE family and by the studies which show that mutation of His160 or Glu230 significantly reduces the catalytic activity of PDE4 (*38*) and PDE5 (*42*). The position of water molecule W3 would lead to an inversion of configuration at phosphorus, consistent with the biochemical studies (*54*, *55*).

The structure of a product-bound PDE4 showed both divalent metal ions interacting with AMP, suggesting a binuclear catalysis. The structure also suggested that a hydroxide ion or a water molecule bridging two metal ions may serve as a nucleophile for the hydrolysis of the phosphoester bond after it is activated by Asp318. Our findings highlight the value of comparisons between the product-bound and unbound enzymes in evaluating the contribution of active site residues and key enzymatic factors such as water molecules and metal ions. Importantly, our results have led to the model for a PDE catalytic mechanism that is founded on direct structural data. Because the elements of the catalytic site are highly conserved among PDE isoforms, the proposed mechanism should be directly applicable to this entire class of enzymes.

ACKNOWLEDGMENT

We thank the 14C beamline staff at APS for assistance with collection of diffraction data.

REFERENCES

1. Houslay, M. D. (1998) *Cell Dev. Biol. 9*, 161−167.
2. Antoni, F. (2000) *Front. Neuroendocrinol. 21*, 103−132.
3. Lucas, K. A., Pitari, G. M., Kazerounian, S., Ruiz-Stewart, I., Park, J., Schulz, S., Chepenik, K. P., and Waldman, S. A. (2000) *Pharmacol. Rev. 52*, 375−414.
4. Klein, C. (2002) *Cell. Signalling 14*, 493−498.
5. Stork, P. J., and Schmitt, J. M. (2002) *Trends Cell Biol. 12*, 258−266.
6. Mehats, C. M., Anderson, C. B., Filopanti, M., Jin, S. L. C., and Conti, M. (2002) *Trends Endocrinol. Metab. 13*, 29−35.
7. Torphy, T. J. (1998) *Am. J. Respir. Crit. Care Med. 157*, 351−370.
8. Conti, M., and Jin, S. L. (1999) *Prog. Nucleic Acid Res. Mol. Biol. 63*, 1−38.
9. Soderling, S. H., and Beavo, J. A. (2000) *Curr. Opin. Cell Biol. 12*, 174−179.
10. Thompson, W. J. (1991) *Pharmacol. Ther. 51*, 13−33.
11. Manganiello, V. C., Taira, M., Degerman, F., and Belfrage, P. (1995) *Cell. Signalling 7*, 445−455.
12. Müller, T., Engels, P., and Fozard, J. R. (1996) *Trends Pharmacol. Sci. 17*, 294−298.
13. Houslay, M. D., and Milligan, G. (1997) *Trends Biochem. Sci. 22*, 217−224.
14. Zhao, A. Z., Yan, C., Sonnenburg, W. K., and Beavo, J. A. (1997) *Adv. Second Messenger Phosphoprotein Res. 31*, 237−251.
15. Houslay, M. D., Sullivan, M., and Bolger, G. B. (1998) *Adv. Pharmocol. 44*, 225−343.
16. Corbin, J. D., and Francis, S. H. (1999) *J. Biol. Chem. 274*, 13729−13732.
17. Francis, S. H., Turko, I. V., and Corbin, J. D. (2001) *Prog. Nucleic Acid Res. Mol. Biol. 65*, 1−52.
18. Corbin, J. D., and Francis, S. H. (2002) *Int. J. Clin. Pract. 56*, 453−459.
19. Giembycz, M. A. (2000) *Drugs 59*, 193−212.

20. Giembycz, M. A. (2002) *Monaldi Arch. Chest Dis. 57*, 48−64.
21. Huang, Z., Ducharme, Y., Macdonald, D., and Robichaud, A. (2001) *Curr. Opin. Chem. Biol. 5*, 432−438.
22. Reilly, M. P., and Mohler, E. R., III (2001) *Ann. Pharmacother. 35*, 48−56.
23. Rotella, D. P. (2002) *Nat. Rev. Drug Discovery 1*, 674−682.
24. Souness, J. E., Aldous, D., and Sargent, C. (2000) *Immunopharmacology 47*, 127−162.
25. Spina, D. (2003) *Curr. Opin. Pulm. Med. 9*, 57−64.
26. Piaz, V. D., and Giovannoni, P. (2000) *Eur. J. Med. Chem. 35*, 463−480.
27. Barnette, M. S., and Underwood, D. C. (2000) *Curr. Opin. Pulm. Med. 6*, 164−169.
28. Sturton, G., and Fitzgerald, M. (2002) *Chest 121*, 192s−196s.
29. Otwinowski, Z., and Minor, W. (1997) *Methods Enzymol. 276*, 307−326.
30. Huai, Q. m., Wang, H., Sun, Y., Kim, H.-Y., Liu, Y., and Ke, H. (2003) *Structure* (in press).
31. Brünger, A.T., et al. (1998) *Acta Crystallogr. D54*, 905−921.
32. Collaborative Computational Project, Number 4 (1994) *Acta Crystallogr. D50*, 760−763.
33. Jones, T. A, Zou, J.-Y., Cowan, S. W., and Kjeldgaard, M. (1991) *Acta Crystallogr. A47*, 110−119.
34. Xu, R. X., Hassell, A. M., Vanderwall, D., Lambert, M. H., Holmes, W. D., Luther, M. A., Rocque, W. J., Milburn, M. V., Zhao, Y., Ke, H., and Nolte, R. T. (2000) *Science 288*, 1822−1825.
35. Dym, O., Xenarios, I., Ke, H., and Colicelli, J. (2002) *Mol. Pharmacol. 61*, 20−25.
36. Jin, S. L., Swinnen, J. V., and Conti, M. (1992) *J. Biol. Chem. 267*, 18929−18939.
37. Pillai, R., Kytle, K., Reyes, A., and Colicelli, J. (1993) *Proc. Natl. Acad. Sci. U.S.A. 90*, 11970−11974.
38. Jacobitz, S., Ryan, M. D., McLaughlin, M. M., Livi, G. P., Dewolf, W. E., Jr., and Torphy, T. J. (1997) *Mol. Pharmacol. 51*, 999−1006.
39. Atienza, J. M., Susanto, D., Huang, C., McCarty, A. S., and Colicelli, J. (1999) *J. Biol. Chem. 274*, 4839−4847.
40. Richter, W., Unciuleac, L., Hermsdorf, T., Kronbach, T., and Dettmer, D. (2001) *Cell. Signalling 13*, 287−297.
41. Zhang, W., Ke, H., Tretiakova, A. P., Jameson, B., and Colman, R. W. (2001) *Protein Sci. 10*, 1481−1489.
42. Turko, I. V., Francis, S. H., and Corbin, J. D. (1998) *J. Biol. Chem. 273*, 6460−6466.
43. Hardman, J. G., Beavo, J. A., Gray, J. P., Chrisman, T. D., Patterson, W. D., and Sutherland, E. W. (1971) *Ann. N.Y. Acad. Sci. 185*, 27−35.
44. Francis, S. H., Colban, J. L., McAllister-Lucas, L. M., and Corbin, J. D. (1994) *J. Biol. Chem. 269*, 22477−22480.
45. Percival, M. D., Yeh, B., and Falgueyret, J. P. (1997) *Biochem. Biophys. Res. Commun. 241*, 175−180.
46. Lohse, D. L., Denu, J. M., and Dixon, J. E. (1995) *Structure 3*, 987−990.
47. Huai, Q., Kim, H. Y., Liu, Y., Zhao, Y., Mondragon, A., Liu, J., and Ke, H. (2002) *Proc. Natl. Acad. Sci. U.S.A. 99*, 12037−12042.
48. Vallee, B. L., and Auld, D. S. (1990) *Biochemistry 29*, 5647−5659.
49. Callahan, S. M., Cornell, N. W., and Dunlap, P. V. (1995) *J. Biol. Chem. 270*, 17627−17632.
50. Omburo, G. A., Jacobitz, S., Torphy, T. J., and Colman, R. W. (1998) *Cell. Signalling 10*, 491−497.
51. Lipscomb, W. N., and Sträter, N. (1996) *Chem. Rev. 96*, 2375−2433.
52. Wilcox, D. E. (1996) *Chem. Rev. 96*, 2435−2458.
53. Thoden, J. B., Philips, G. N., Neal, T. M., Raushel, F. M., and Holden, H. M. (2001) *Biochemistry 40*, 6989−6997.
54. Burgers, P. M. J., Eckstein, F., Hunneman, D. H., Haraniak, J., Kinas, R. W., Lesiak, K., and Stec, W. J. (1979) *J. Biol. Chem. 254*, 9959−9961.
55. Coderre, J. A., Mechdi, S., and Gerlt, J. A. (1981) *J. Am. Chem. Soc. 103*, 1872−1875.
56. Houslay, M. D., and Adams, D. R. (2003) *Biochem. J. 370*, 1−18.

BI034653E